

Orientation dependence in near-field scattering from TiO₂ particles

L. E. McNeil, A. R. Hanuska, and R. H. French

This scattering of light by small particles embedded in a continuous transparent medium is influenced not only by the bulk optical properties of the particles and the medium but also by the size, shape, and spatial arrangement of the particles—that is, by the microstructure. If the particles are close together, as in agglomerated coatings or stereolithographic suspensions, interactions between the radiation fields of adjacent particles can lead to variations in the magnitude and spatial arrangement of the scattered light in the near and the far field, which can affect the color and hiding power of a coating, the cure depth and homogeneity in stereolithography, and the threshold intensity for stimulated emission in random lasers. Our calculations of the near- and the far-field scattering distribution for 200-nm TiO₂ spheres in pairs of various orientations and in an ordered array of five particles show that, depending on the orientation of the particles with respect to the incident light, these interactions can either increase or decrease the scattering efficiency, the isotropy of the scattering, and the magnitude of the electric field strength within the matrix and the particles. In the mid-visible range, two particles in line increase the backscattering fraction by 28% and the scattering strength by 38% over that of a single particle, whereas if the particles are in the diagonal configuration the backscattering fraction and scattering strength are actually reduced by addition of the second particle. At shorter or longer wavelengths the backscattering fraction is reduced regardless of the location of the second particle, by as much as 60% when five particles are arranged in the zigzag configuration. These results are surprising in that it is generally assumed that multiple scattering enhances backscattering. Simple models of multiple scattering or scattering of two particles as a single, larger particle are inadequate to explain these results. © 2001 Optical Society of America

1. Introduction

The scattering of light by small particles in a continuous matrix is of considerable relevance to a variety of applications such as coatings, stereolithography, lasing in random media, and photonic solids. This scattering is determined not only by the bulk optical properties of the particles and the medium but also by the size, shape, and spatial arrangement of the particles—that is, by the microstructure. The scattering can be strongly influenced by inhomogeneities in the random microstructure, such as agglomeration and the development of ordered arrays of particles.¹ If the particles are separated by distances compara-

ble with their diameter, as is the case for high particle concentrations or agglomerated systems, the near-field interactions between the radiation fields of the particles can strongly influence the resulting far-field electric field distribution and thus the appearance and hiding power of a coating. Variations in electric field in the near field directly influence the depth and uniformity of the curing in stereolithography, and the threshold electric field strength for stimulated emission in random media. The near-field variations also determine the localization of photons and thus the existence of optical stop bands. It is therefore of considerable importance to determine the effects of changes in the local arrangements of the particles, i.e., in the microstructure, on both the near- and the far-field scattering of light. Because it is difficult to access this information experimentally, we employed computational methods.

For single particles of simple shapes it is possible to calculate analytically the magnitude of the electric field of the scattered light in the far field, with approaches such as Mie theory.^{2,3} If the particles are sufficiently far apart that the scattered radiation

L. E. McNeil (mcneil@physics.unc.edu) is with the Department of Physics and Astronomy, University of North Carolina at Chapel Hill, Chapel Hill, North Carolina 27599-3255. A. R. Hanuska and R. H. French are with DuPont Central Research and Development, Wilmington, Delaware 19880-0356.

Received 6 November 2000; revised manuscript received 28 March 2001.

0003-6935/01/223726-11\$15.00/0

© 2001 Optical Society of America

from the different particles can be added incoherently, then the scattering can be completely described by this analysis. In many applications of light scattering, in particular, in paints, pigments, and coatings as well as in stereolithography, the particles are sufficiently close together that their radiation fields interact. In this case the scattering from one particle is affected by the adjacent particles, and the assumption of independent scatterers no longer holds. Thus the near-field radiation pattern becomes crucial, because it determines the interaction of the radiation fields of the particles with one another and therefore both the local scattered electric field strength (important for stereolithography) and the far-field electric field distribution (important for coatings).

Mie theory, though exact for the particular case of a single optically isotropic spherical particle in a non-absorbing medium, is not easily extended to the realistic situation of multiple, irregularly shaped, interacting particles in an absorbing medium. Mie theory in its simplest applications also addresses only the far-field irradiance, and it is difficult to extract information about the near-field electric field distributions that are crucial in understanding the interactions of closely spaced particles. To calculate the scattering for multiple interacting particles, it is necessary to abandon the analytic approach and instead use numerical methods. This can be done with a finite-element method, in which the volume containing the scatterers and the medium is divided up into discrete regions that are small compared with the wavelength and the particle size. Maxwell's equations are then solved in each region for a given incident wave by use of the appropriate optical constants for the material of which the region is composed. We can then extrapolate the obtained near-field solution to the far field by simply allowing it to propagate through a uniform medium. This technique can in principle be used to calculate the scattering from any number of arbitrarily shaped, inhomogeneous, optically anisotropic particles, in any configuration, if the necessary computing power is available.

This technique has been previously applied to individual particles and small clusters of TiO_2 in resin and latex in water,⁴⁻⁶ at a single wavelength for which the absorption of light by the particles is negligible. Single quinacridone pigment particles and pairs of particles in different configurations for wavelengths across the visible spectrum have been considered as well.⁷ Here we consider single and multiple TiO_2 spheres in resin at three wavelengths in the visible-light range. These wavelengths include both the strongly absorbing and the transparent regions.

As in our previous research, we have chosen a particle size in the resonant regime, in which the diameter is comparable with the wavelength of light in the medium. Specifically, for 200-nm TiO_2 in resin, the size parameter $x = 2\pi a n_{\text{resin}}/\lambda$, where a is the diameter of the particle; λ is the wavelength of light in vacuum; and n_{resin} is the refractive index of the resin at λ , is in the range $2 < x < 8$. In this regime the

scattering is strong, especially when weighted by the volume of the particle. The scattered light from a single particle is also strongly forward directed, with no more than 30% of the scattered light appearing in the backward hemisphere.

At $\lambda = 250$ nm for the single particle we performed the calculation for two cases: (i) with realistic values for index of refraction and absorption coefficient of the particle and the medium and (ii) with the absorption of the particle artificially set to zero. This second case is of course not physically realizable, since the index of refraction and the absorption coefficient are linked through the Kramers-Kronig relations and cannot be changed independently. However, the nonphysical situation does allow us to examine explicitly the effects of absorption, i.e., the loss of light from the radiation field, independent of effects that are due to the magnitude of the wavelength relative to the particle diameter.

To examine the interactions between the radiation fields of adjacent particles, we performed the calculations for pairs of particles with a surface-to-surface distance $L = 75$ nm. We placed the pairs of particles in three orientations with respect to the direction of the incident light: (i) with the line joining the centers of the particles parallel to the incident direction (the in-line configuration), (ii) with the line perpendicular to that direction (the side-by-side configuration), and (iii) with the line at a 45° angle from the incident direction (the diagonal configuration). Our earlier calculations⁷ for quinacridone pigment particles showed that the orientation of the particles relative to the incident direction has a significant effect on the far-field scattering parameters as well as on the near-field electric field distribution.

We also performed the calculation for a single staggered arrangement of five particles in two rows, with the line joining the particles in each row perpendicular to the incident direction. The particles within each row are thus in the side-by-side configuration. The two particles in the second row (i.e., the row that the incident light encounters second) are placed between the pairs of particles in the first row, forming a zigzag arrangement in which the particles in the second row are in the diagonal configuration with respect to those in the first.

2. Calculation Methods

TiO_2 is birefringent, with a different index of refraction for light polarized perpendicular or parallel to the optic axis. In all these calculations the average-index approximation was used. In this approximation the TiO_2 particle is assumed to be isotropic, with real and imaginary parts of the refractive index equal to $n_{\text{particle}} = (2n_o + n_e)/3$ and $k = (2k_o + k_e)/3$. Earlier studies⁵ have shown that this approximation reproduces the scattering of the optically anisotropic sphere of this diameter quite well. The values for the optical constants were taken from the literature,⁸ with linear interpolation applied where the value for the desired wavelength was not available. The optical constants as a function of wavelength for the

resin in which the particles are embedded were taken from ellipsometric measurements of a typical resin (without particles) used in automotive coatings. The real index of this resin ranges from $n_{\text{resin}} = 1.5959$ at $\lambda = 250$ nm to 1.4448 at $\lambda = 850$ nm, and its absorption coefficient is negligible in this wavelength range.

The finite-element method adopted in this study to compute the electromagnetic radiation scattering of single- and multiple-particle films uses the program EMPLEX (Weidlinger Associates, Incorporated). It is based on piecewise solutions of the time-domain form of Maxwell's equations in source-free space given in Eq. (1), where the computational domain is discretized into a finite number of volume elements. In Eq. (1), E is the electric field amplitude, ϵ the electric permittivity of the medium, and μ the magnetic permeability of the medium:

$$\nabla^2 E - \epsilon\mu \frac{\partial^2 E}{\partial t^2} = 0. \quad (1)$$

The parameters required for constructing the finite-element models used throughout this study consist of the edge dimensions in a Cartesian coordinate system, the finite-element mesh density, the particle positions, the particle shapes, and the wavelength-dependent optical properties of the materials contained in the model. The number of elements in a particular model varies according to the edge dimensions and the mesh density. Typical models contain between 5 and 10 million elements. A plane wave of circularly polarized electromagnetic radiation is propagated through the model in the time domain while the nodal electric and magnetic fields and amplitudes are computed at each time step. The magnitude squared of the resulting total and scattered electric field are available at each node for every time step; however, only steady-state results are of interest in this study. The values of the squared magnitudes of the electric fields given in Figs. 1–3 are relative to the incident wave. To obtain the far-field scattered electric field magnitudes, the near-field scattered waves are extrapolated onto the surface of a far-field sphere with a radius of 150 μm , which is large compared with the wavelength of the electromagnetic radiation.

Once the far-field scattered electric field has been extrapolated, macroscopically observable physical quantities such as the scattering cross section C_{sca} of the angular distribution of the scattered light can be computed. The scattering cross section C_{sca} defined in Eq. (2) is expressed in units of area, where θ is the scattering angle, I_0 is the squared magnitude of the electric field of the incident radiation, and $I_{\text{sca}}(\theta)$ is the same quantity for the scattered wave on the surface of the far-field sphere over which the surface integral is performed:

$$C_{\text{sca}} = \frac{1}{I_0} \int_{4\pi} I_{\text{sca}}(\theta) d\Omega. \quad (2)$$

The scattering coefficient S is defined as the scattering cross section normalized by the volume of the scattering material in the model. In Eq. (3) the scattering coefficient S is expressed in units of inverse length:

$$S = C_{\text{sca}}/V. \quad (3)$$

In addition to the finite-element calculations that form the bulk of this study, we also performed some analytical calculations of far-field scattering from single spheres, using Mie theory. In these calculations we used the programs BHMIE³ and MIETAB.⁹

3. Results

A. Short-Wavelength, High-Absorption Region ($\lambda = 250$ nm)

At the shortest wavelength considered, $\lambda = 250$ nm, where the particle's refractive index $n_{\text{particle}} = 2.25$, its absorption $k = 1.43$, and the Mie size parameter $x = 8.0$, the scattered field forms a plume in the forward-scattering direction (scattering angle $\theta = 0$). This can be seen in Fig. 1(a). The plume is roughly cylindrical, approximately 190 nm across and extending approximately 370 nm away from the particle surface. At the particle surface at $\theta = 0$ there is a shallow local minimum, and the maximum electric field magnitude occurs at $\theta = 0$ approximately 40 nm from the particle surface. At this point the scattered field magnitude is 1.5 times that of the incident wave. The maximum value of the squared electric field magnitude within the particle is approximately 1.2 times that of the incident wave.

In this wavelength region the wavelength of the light is comparable with the diameter of the particle. Of the wavelength regions explored in this study, it is thus the closest to the geometrical optics regime. However, in that regime, the maximum electric field strength would occur approximately 70 nm from the particle surface, rather than at a little more than half that distance.

In the far field the scattered light is likewise strongly forward directed, with half the scattered light appearing in a cone of half-angle 20° centered on $\theta = 0$. The scattering cross section $C_{\text{sca}} = 0.040 \mu\text{m}^2$, and the extinction cross section $C_{\text{ext}} = C_{\text{sca}} + C_{\text{abs}} = 0.082 \mu\text{m}^2$, where C_{abs} is the absorption cross section.

Only at this short wavelength are the effects of absorption in the TiO_2 particle observable. The most striking effect of turning off the absorption in the particle is to shift the location of the dominant portion of the scattered electric field strength from a plume distributed downstream of the particle to a location inside the particle, ~ 10 nm from its surface. Removing the absorption also increases the magnitude of the field strength maximum by a factor of more than 10, to 15.7 times the value for the incident wave. In the far field the scattering in the absence of absorption directs half the light into a cone with a somewhat larger half-angle (23° versus 20°), but less

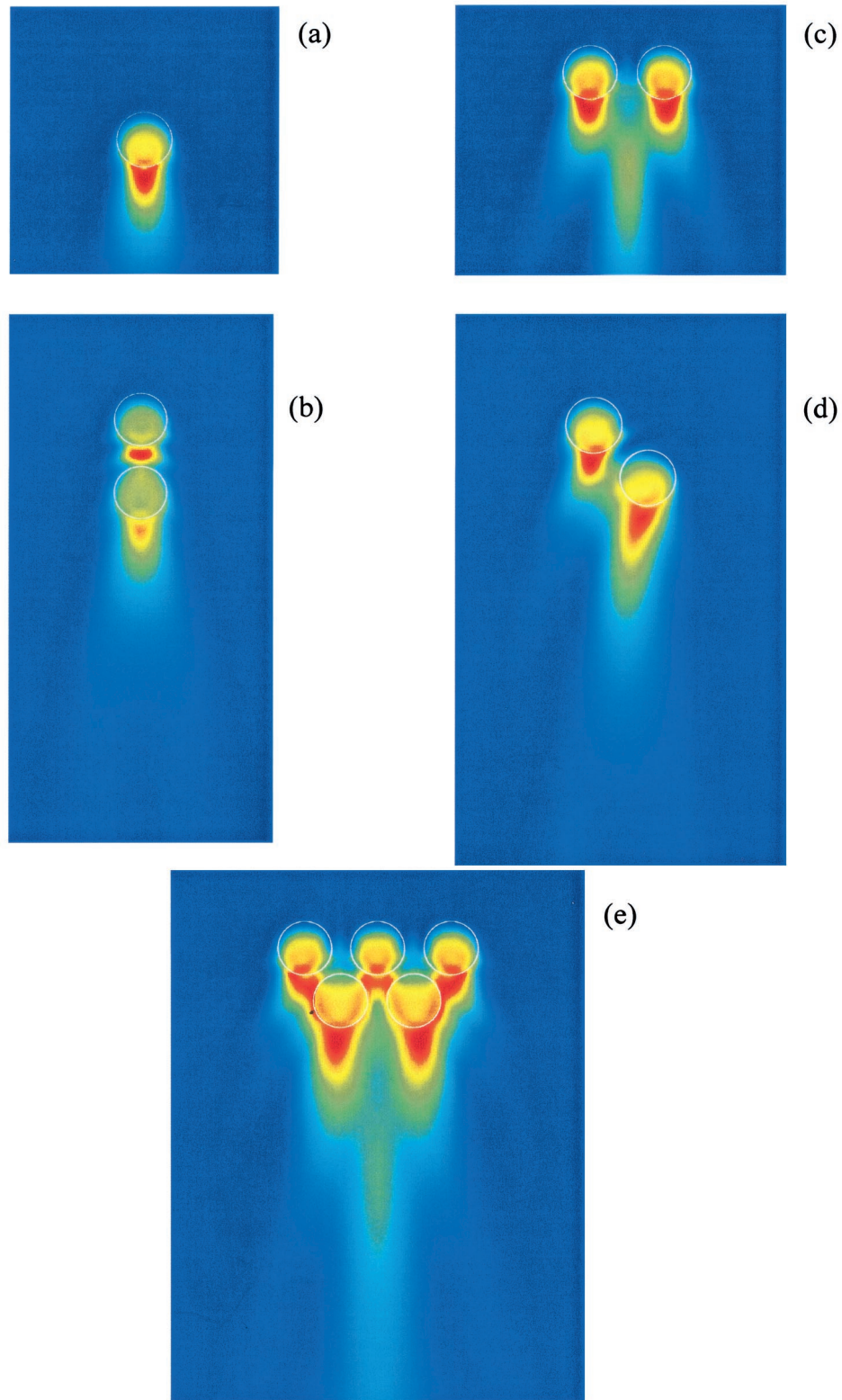


Fig. 1. Near-field values of the square of the electric field magnitude of the scattered wave for 200-nm TiO_2 particles illuminated by 250-nm light. The images show a cross-section in the plane containing the incident direction and the particle center. The light is incident from the top edge of each image. All values are relative to the incident wave. (a) Single particle; spatial dimension $1 \mu\text{m} \times 1 \mu\text{m}$; scale 1.50 (red) to 5.47×10^{-4} (blue). (b) In-line configuration; spatial dimension $1 \mu\text{m} \times 2 \mu\text{m}$; scale 1.78 (red) to 5.94×10^{-4} (blue). (c) Side-by-side configuration; spatial dimension $1.25 \mu\text{m} \times 1 \mu\text{m}$; scale 1.39 (red) to 5.74×10^{-4} (blue). (d) Diagonal configuration; spatial dimension $1.25 \mu\text{m} \times 2 \mu\text{m}$; scale 1.50 (red) to 2.11×10^{-5} (blue). (e) Zigzag configuration; spatial dimension $1.5 \mu\text{m} \times 2 \mu\text{m}$; scale 1.40 (red) to 3.76×10^{-4} (blue).

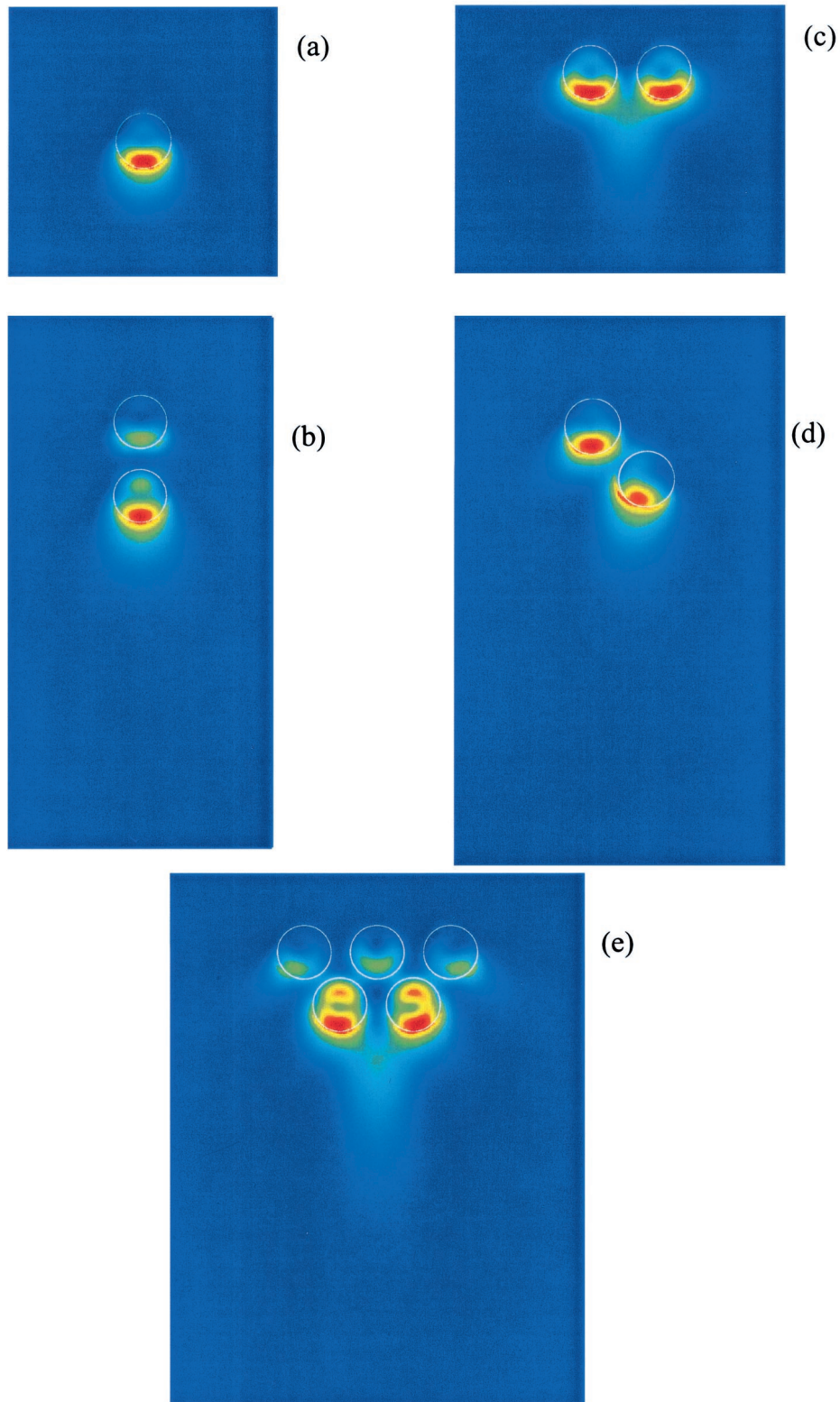


Fig. 2. Near-field values of the square of the electric field magnitude of the scattered wave for 200-nm TiO_2 particles illuminated by 550-nm light. The images show a cross section in the plane containing the incident direction and the particle center. The light is incident from the top edge of each image. All values are relative to the incident wave. (a) Single particle; spatial dimension $1 \mu\text{m} \times 1 \mu\text{m}$; scale 4.19 (red) to 1.05×10^{-3} (blue). (b) In-line configuration; spatial dimension $1 \mu\text{m} \times 2 \mu\text{m}$; scale 8.91 (red) to 5.19×10^{-4} (blue). (c) Side-by-side configuration; spatial dimension $1.25 \mu\text{m} \times 1 \mu\text{m}$; scale 4.21 (red) to 3.32×10^{-3} (blue). (d) Diagonal configuration; spatial dimension $1.25 \mu\text{m} \times 2 \mu\text{m}$; scale 4.22 (red) to 6.50×10^{-4} (blue). (e) Zigzag configuration; spatial dimension $1.5 \mu\text{m} \times 2 \mu\text{m}$; scale 9.44 (red) to 2.69×10^{-4} (blue).

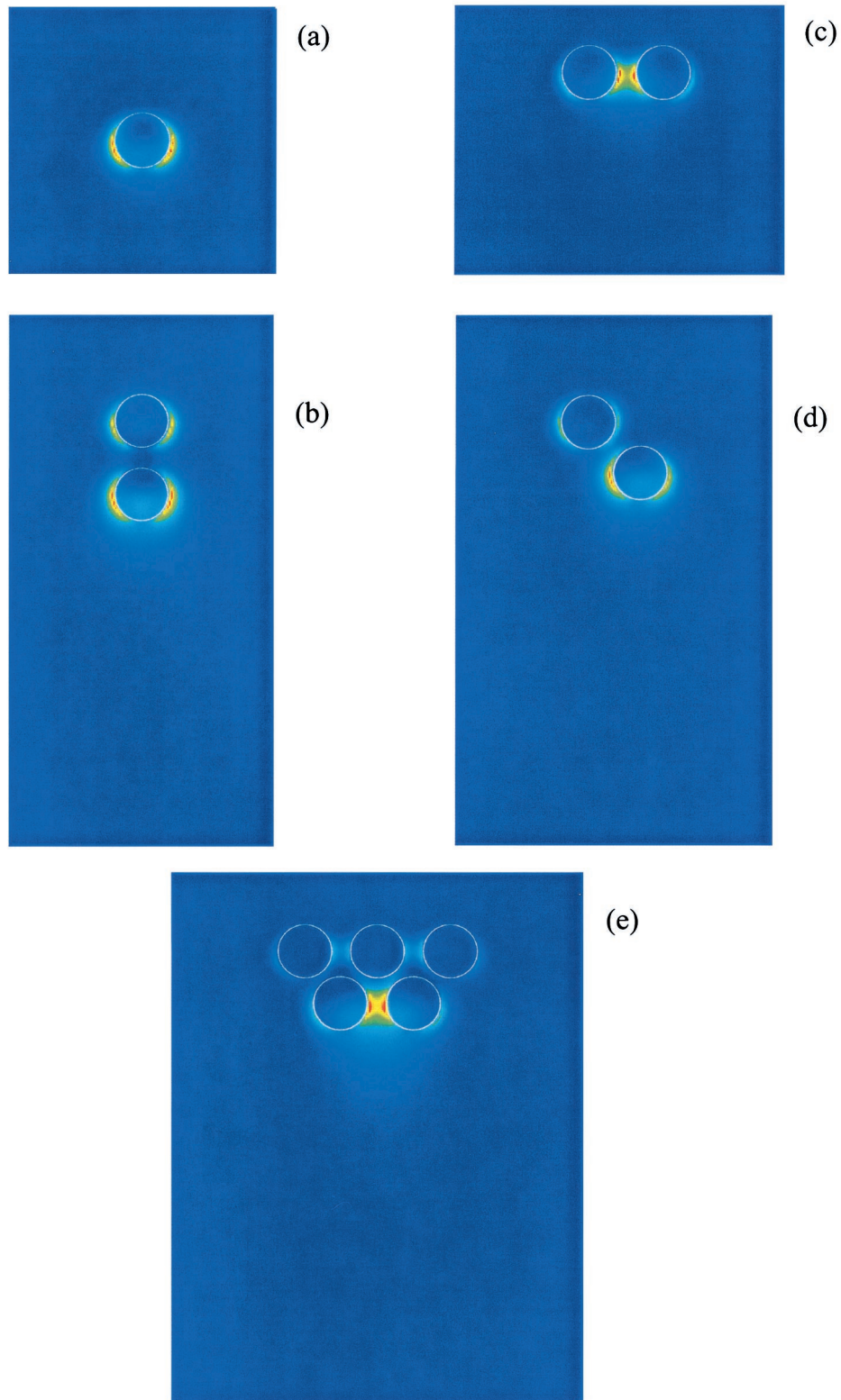


Fig. 3. Near-field values of the square of the electric field magnitude of the scattered wave for 200-nm TiO_2 particles illuminated by 850-nm light. The images show a cross-section in the plane containing the incident direction and the particle center. The light is incident from the top edge of each image. All values are relative to the incident wave. (a) Single particle; spatial dimension $1 \mu\text{m} \times 1 \mu\text{m}$; scale 0.931 (red) to 1.82×10^{-3} (blue). (b) In-line configuration; spatial dimension $1 \mu\text{m} \times 2 \mu\text{m}$; 1.53 (red) to 1.32×10^{-3} (blue). (c) Side-by-side configuration; spatial dimension $1.25 \mu\text{m} \times 1 \mu\text{m}$; 1.73 (red) to 3.70×10^{-4} (blue). (d) Diagonal configuration; spatial dimension $1.25 \mu\text{m} \times 2 \mu\text{m}$; scale 1.58 (red) to 5.11×10^{-4} (blue). (e) Zigzag configuration; spatial dimension $1.5 \mu\text{m} \times 2 \mu\text{m}$; scale 3.81 (red) to 3.59×10^{-4} (blue).

of the scattered light is directed into the backward hemisphere (4.5% versus 6.5%). A more striking difference is in the scattering cross section. For the nonabsorbing case, $C_{\text{sca}} = C_{\text{ext}} = 0.115 \mu\text{m}^2$, 40% larger than for the particle with absorption.

With two particles in the in-line configuration, the surface of the second particle lies 75 nm downstream of the surface of the first, placing it within the scattering plume of the first particle. In this case the scattered field forms a hot spot between the particles, approximately 30 nm from the first particle, as can be seen in Fig. 1(b). The squared magnitude of the electric field at this point is 1.78 times that of the incident wave, which is higher than the maximum value for the single-particle case. Because of constructive interference, the scattering from the second particle has enhanced the total scattered wave downstream of the first. At this wavelength the spacing between the particle surfaces is close to $\lambda/2n_{\text{resin}}$. In the extended region downstream of the second particle, a scattering plume similar to that for the single particle is present, though the shadowing of the first particle reduces the maximum electric field magnitude in the center of the plume somewhat. Within the particles the squared electric field magnitude is no larger than 1.2 times the value for the incident wave.

In the side-by-side configuration each particle produces a scattering plume that extends approximately 275 nm downstream of the particle surface, similar to the single-particle case. As Fig. 1(c) shows, the two plumes then abruptly join to form a single plume centered between the two particles, approximately 200 nm wide and extending more than 650 nm away from the particle surfaces. The maximum squared electric field magnitude in the individual plumes, located approximately 25 nm from the surface of each particle, is 1.39 times the incident value for the incident wave, somewhat lower than for the single particle. The maximum value in the central plume formed downstream of the two particles is approximately 0.75 times the incident value. Within the particles the maximum value does not exceed 1.2 times the incident value.

In the diagonal configuration, shown in Fig. 1(d), the particles again each produce a scattering plume similar to that for the single-particle case, but the axes of the plumes are directed approximately 15° from the forward direction, away from the line joining the centers of the particles. The maximum scattered squared electric field magnitude of 1.50 times the incident value occurs in the plume produced by the first particle, with the hot spot in the second plume having slightly lower value. The second plume extends approximately 500 nm beyond the surface of the second particle, considerably farther than in the single-particle case. Within the particles, the maximum value does not exceed 1.1 times the incident value.

In the five-particle zigzag array the scattered light forms bridges between the particles in the first row and those in the second. As can be seen in Fig. 1(e),

the maximum squared electric field magnitude in these bridges is similar to that found in the plumes extending downstream of the second row, or ~ 1.40 times the incident value. Within the particles, the maximum value does not exceed 1.2 times the incident value. As in the side-by-side case, the plumes from the two particles abruptly join to form a single, central plume beginning approximately 360 nm downstream of the particle surfaces, with the central plume extending to approximately 1220 nm from the surfaces. However, unlike in the two-particle side-by-side case, each of the plumes is asymmetrical about its central axis, extending farther in the direction away from the other particle in the row than in the direction between the two particles. This consequence of the interference between the two scattered fields mimics a slight repulsion of the each plume by the other. The presence of additional particles thus has several effects: The scattered field between the particles is enhanced over the diagonal case, the scattered plume extends farther from the particles, and the symmetry of the plumes is modified.

B. Intermediate-Wavelength, High-Scattering Region ($\lambda = 550 \text{ nm}$)

At this wavelength the absorption coefficient of TiO_2 is negligible, $n_{\text{particle}} = 2.74$, and $x = 3.4$. The index contrast $m = n_{\text{particle}}/n_{\text{resin}}$ has its largest value for the wavelengths considered, 1.83 compared with 1.41 at 250 nm and 1.80 at 850 nm. Consistent with what we observed at 250 nm with the absorption turned off, the scattered squared electric field magnitude is primarily found within the particle [Fig. 2(a)]. The maximum in the scattered value is located approximately 30 nm from the surface of the particle, nearest the side opposite from that at which the light is incident, with a magnitude of 4.19 times the incident value. Outside the particle (but near its surface) the scattered light develops a toroidal shape, with a local minimum at $\theta = 0$. The light is much less concentrated in the forward direction than at the shorter wavelength, with significant scattered electric field strength at scattering angles approaching 90° . In the far field the light is also less forward directed, with half the scattered light appearing in a cone of half-angle 15° and 13.5% of the scattered light being directed into the backward hemisphere. The scattering cross section $C_{\text{sca}} = 0.109 \mu\text{m}^2$, similar to the nonabsorbing case at 250 nm.

In the in-line configuration [Fig. 2(b)], the scattered light is concentrated in the second particle, with the maximum scattered squared electric field magnitude occurring approximately 20 nm inside the surface on the side opposite that where the light is incident. The value at that point is 8.91 times the incident value, more than twice as large as for the single particle. Thus any process occurring within the TiO_2 particle, such as photoemission, would be enhanced by the presence of a second particle in this orientation. Unlike at $\lambda = 250 \text{ nm}$, the electric field strength between the two particles is low. Two secondary maxima also appear, one in the first particle

and one in the second. At a vacuum wavelength of 550 nm the wavelength of light in the particle is nearly equal to the particle diameter, so interference effects are to be expected. Similar to the case of the single particle, the scattered squared electric field magnitude outside the second particle is concentrated near its surface and is distributed over a wider range of scattering angles than at shorter wavelengths.

When the two particles are side by side [Fig. 2(c)], the scattered light within each particle resembles the single-particle case. However, outside the particles the two distributions of scattered light join together, making a weak central plume that extends approximately 200 nm downstream of the particle surfaces. The maximum value is approximately that of the single-particle case.

For the diagonal arrangement [Fig. 2(d)] the scattering distribution of the second particle is skewed by the presence of the first and extends to larger scattering angles on the side of the sphere closest to the first particle. The distribution of light scattered from the first particle is much less affected, and the maximum value (which occurs within the first particle) is approximately the same as for the single particle.

The five-particle zigzag arrangement [Fig. 2(e)] gives a scattering pattern that is similar to the side-by-side arrangement. The scattered light is concentrated within the particles on the second row, and the maximum in the scattered squared electric field magnitude is 9.44 times the incident value, or approximately double that of the other configurations (except the in-line configuration, with which it is comparable). The central plume extends approximately 245 nm from the surfaces of the second row of particles.

C. Long-Wavelength Region ($\lambda = 850$ nm)

At $\lambda = 850$ nm, $n_{\text{particle}} = 2.60$ and $x = 2.1$. The scattered light in the near field is now almost entirely contained within a torus centered on the forward direction, confined to angles $55^\circ < \theta < 90^\circ$ [Fig. 3(a)]. Essentially none of the scattered light is found within the particle. The maximum value of the scattered squared electric field magnitude is only 0.93 times the incident value, and the maximum is located near the particle surface. The far-field values reflect this change, with half the scattered light directed into a cone of half-angle 63° and 30% of the scattered light directed into the backward hemisphere. This decrease in the anisotropy of the scattering pattern as the wavelength of the light increases relative to the particle diameter (or, equivalently, as the Mie size parameter decreases) is a familiar result. The scattering in the far field also becomes weaker, with $C_{\text{sca}} = C_{\text{ext}} = 0.021 \mu\text{m}^2$, only 20% of the value at 550 nm.

The distribution of scattered light in the in-line case [Fig. 3(b)] resembles that of a single particle, with a toroid at the surface of each particle. The toroid on the second particle is more pronounced than that on the first, with a maximum squared electric field magnitude that is 1.53 times the incident value.

The scattered light between the particles is negligible.

In the side-by-side configuration [Fig. 3(c)], essentially all the scattered light is found between the particles, forming a bridge between them on the line joining their centers. The maximum squared electric field magnitude occurs outside the spheres, close to their surfaces on the line joining their centers, and with a value of 1.73 times the incident value.

In the diagonal configuration [Fig. 3(d)], the scattered distribution resembles that of the in-line configuration, in that the scattered light is confined to a toroid at the surface of each particle, with the squared electric field magnitude being greater near the second particle. However, the second particle's toroid is skewed toward the first particle so that the maximum value (1.58 times the incident value) is located on that side.

The scattering pattern for the zigzag arrangement [Fig. 3(e)] strongly resembles that of the side-by-side arrangement. The scattered light is concentrated almost entirely between the two particles in the second row on the line joining their centers, with a maximum squared electric field magnitude of 3.81 times the incident (and thus approximately twice that for the side-by-side arrangement).

4. Discussion

A. Near-Field Interactions

If the interparticle spacing $L = 75$ nm used here represented the average spacing between particles, the particle volume concentration would be 38.5%, which is higher than would be found in a typical coating but lower than that of a stereolithographic suspension. However, if the particles are not evenly dispersed, so that spacings smaller (and larger) than the average occur with high frequency (as would be the case if agglomeration were not prevented), such close approaches of particles to one another are likely to occur even in coatings and would influence the light-scattering characteristics of the resulting structure. This spacing is one-eighth to one-half the wavelength of light in the resin, so interaction of the radiation fields of adjacent particles is expected to affect the scattering in both the near and the far field.^{4,6} It is clear from the results described above and displayed in Figs. 1–3 that the orientation of the particles with respect to the direction of the incident light strongly affects the distribution of the scattered light. The variation in squared electric field magnitude of the scattered light at short wavelengths in the matrix near the particles (from 1.78 times the incident value to negligible values; see Fig. 1) could lead to inhomogeneity of curing in stereolithography. The local electric field strength of the scattered light within the particle is also important in the photoemission-induced degradation of a coating. The doubling of the squared electric field magnitude within the second particle in the in-line configuration at $\lambda = 550$ nm compared with the side-by-side or diagonal arrangements would tend to accelerate such

Table 1. Scattering Parameters for Single and Multiple 200-nm TiO₂ Particles from EMFLEX Calculations^a

Wavelength (nm)	Absorption	Parameters	Single Particle	In Line	Side by Side	Diagonal	Zigzag
250	1.43	<i>B</i> (%)	6.5	4.1	5.0	3.9	3.7
		<i>C</i> _{sca} (μm ²)	0.40	0.073	0.083	0.096	0.180
		<i>S</i> (μm ⁻¹)	9.506	8.661	9.948	11.431	8.611
550	0.00	<i>B</i> (%)	13.5	19.0	14.9	12.5	13.5
		<i>C</i> _{sca} (μm ²)	0.109	0.303	0.231	0.196	0.628
		<i>S</i> (μm ⁻¹)	26.129	36.125	27.614	23.377	29.965
850	0.00	<i>B</i> (%)	30.1	25.5	26.8	20.4	12.5
		<i>C</i> _{sca} (μm ²)	0.021	0.068	0.044	0.060	0.176
		<i>S</i> (μm ⁻¹)	5.018	8.065	5.255	7.119	8.412

^aBackscattering fraction *B*, scattering cross section *C*_{sca}, and volume-normalized scattering parameter *S*.

degradation, and the even higher values in the zigzag configuration would enhance this tendency. While in a random distribution of particles all of the configurations would be expected to be equally likely and to contribute to the total field, this would not be the case in a nonrandom distribution. Such a textured distribution might be produced resulting from the influence of a surface or some anisotropy introduced in processing. Deliberate manipulation of the microstructure to create optical stop bands may also be possible.

B. Scattering in the Far Field

The far-field scattering parameters for each of the wavelengths and particle configurations are given in Table 1. The scattering cross section *C*_{sca} is the integral of the scattered squared electric field magnitude over the entire far-field sphere, and the volume-normalized scattering parameter *S* = *C*_{sca}/*V* where *V* is the volume of TiO₂ present. The backscattering fraction *B* is the fraction of the total scattered field that is directed into the backward hemisphere (scattering angle >90°). Since backscattering is typically a desirable characteristic in a coating, particle interactions that reduce this quantity are of particular interest in that application.

To interpret these results, we consider some simple models. If the particles were to act as single, totally independent scatterers (as would be the case if they were separated by distances large compared with their diameter and with the wavelength), the scattered electric fields would be purely additive. *C*_{sca} would scale with the number of particles, and *S* and *B* would remain constant as particles were added. If the particles were to behave as single scatterers, but multiple scattering were to occur, both *S* and *B* would be expected to increase as particles were added. In this model, light that was not scattered by the first particle could be scattered by the second, and light scattered by the first particle could be incident on the second particle at angles other than θ = 0 and thus be directed to larger scattering angles by the second scattering event. In both cases the qualitative behavior would be independent of wavelength. Table 1 shows that neither of these simple models is adequate to explain the results.

If the two or more particles were to scatter light as if they formed a single, larger particle, the effect on the scattering would depend on the wavelength. As can be seen in Fig. 4, which displays the results of Mie theory calculations of the volume-normalized scattering parameter *S* for single TiO₂ spheres of various diameters, the single 200-nm TiO₂ particle is larger than optimal size for 250-nm light; i.e., it has a smaller *S* than would a particle with a smaller diameter. For 850-nm light *S* has maxima at *a* = 320 and 440 nm, so a 200-nm particle is of suboptimal size. For 550-nm light it is nearly optimal, since the curve of *S* versus *a* has maxima of nearly equal magnitude at *a* = 190 and 270 nm.

Like *S*, the backscattering fraction *B* for a single particle depends on wavelength as well as particle diameter. In general, particles that are small relative to the wavelength have a more isotropic scattering distribution and thus a larger value of *B* than do larger particles. However, for diameters comparable with the wavelength, *B* displays pronounced oscillations as a function of diameter, especially for wavelengths for which the absorption of light in the particle is negligible. Mie theory calculations of *B* versus *a* for single particles can be seen in Fig. 5.

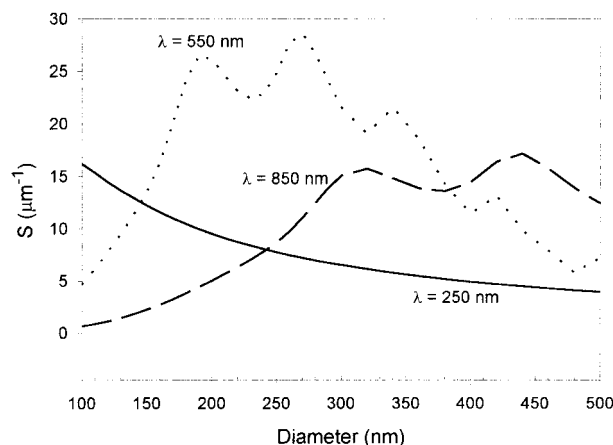


Fig. 4. Volume-normalized scattering parameter *S* versus particle diameter for single TiO₂ particles at various wavelengths, calculated with Mie theory. Solid curve, λ = 250 nm; dotted curve, λ = 550 nm; dashed curve, λ = 850 nm.

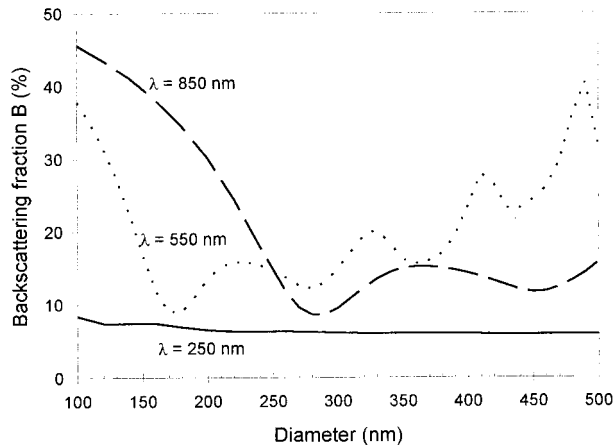


Fig. 5. Backscattering fraction B versus particle diameter for single TiO_2 particles at various wavelengths, calculated with Mie theory. Solid curve, $\lambda = 250$ nm; dotted curve, $\lambda = 550$ nm; dashed curve, $\lambda = 850$ nm.

These curves show that, as a increases, the backscattering fraction at $\lambda = 250$ nm declines slightly. At $\lambda = 550$ nm the backscattering fraction oscillates around a general upward trend for $a > 170$ nm, so that larger particles (or groups of small particles scattering like a single, larger particle) would tend to have a similar or somewhat larger value of B . At $\lambda = 850$ nm B decreases as a increases to 280 nm and thereafter oscillates about a slow upward trend.

The values of S and B for single particles with volume equivalent to two and five 200-nm spheres are shown in Table 2. Although the values in Table 2 capture some of the behavior shown in Table 1 for pairs and quintuplets of particles, the orientation dependence of the data in Table 1 shows that this model is also too simple to explain the results obtained here. For example, at $\lambda = 250$ nm, S is larger for the side-by-side and diagonal pairs of particles than for the single particle, where a smaller value would be expected if the two particles acted as one. However, for the same configurations (as for the others at this wavelength), the backscattering fraction is smaller than for the single particle; i.e., the effect of the additional particle is to make the scattering more forward directed. Yet for the in-line and zigzag configurations at this wavelength, S (as well as B) is reduced by the additional particle(s); thus adding

Table 2. Volume-Normalized Scattering Parameters S and Backscattering Fraction B for Single TiO_2 Particles, Calculated from Mie Theory^a

Wavelength (nm)	Diameter, 252 nm		Diameter, 342 nm	
	S (μm^{-1})	B (%)	S (μm^{-1})	B (%)
250	7.669	6.3	5.719	6.0
550	25.420	14.5	21.691	17.9
850	8.855	14.1	14.662	14.6

^aA particle with diameter of 252 nm has a volume equivalent to two 200-nm particles, and a 342-nm particle is equivalent in volume to five such particles.

particles in those configurations reduces the effectiveness of the scattering from each particle.

One might expect a monotonic change in both S and B as the position of the second particle is changed from the in-line to the diagonal to the side-by-side configuration. However, this is true only for S at $\lambda = 850$ nm. At $\lambda = 550$ nm, S decreases as the second particle is moved from the in-line to the diagonal position and then increases as it is moved to the side-by-side position. At $\lambda = 250$ nm the opposite is true. Thus, at this interparticle spacing, whether or not multiple scattering is more efficient (in the sense of a larger S) than single scattering depends in a complicated way on the orientation of the particles with respect to the direction of the incident light and on the wavelength of the light. For the backscattering fraction B the picture is slightly simpler in that B decreases at all wavelengths as the second particle is moved from the in-line to the diagonal configuration, and then it increases as it is moved to the side-by-side configuration.

The zigzag configuration has characteristics of both the side-by-side and the diagonal configurations, but the values of S and B do not reflect that similarity. This is particularly noticeable at $\lambda = 850$ nm, where the addition of three more particles to either the diagonal or side-by-side configuration causes S to increase and B to decrease; i.e., the scattering becomes more efficient but also more forward directed. The decrease in B is particularly striking in light of Fig. 5 (or Table 2), which would predict that B would be little changed over this volume range.

In a random arrangement of particles the probability that a pair of particles will have a particular orientation with respect to the direction of the incident light will be proportional to the fraction of the volume available for the second particle to occupy that corresponds to that orientation. If a system of spherical coordinates is adopted with its origin at the center of the first particle and the polar axis defined by the direction of the incident light, then the in-line configuration would place the center of the second particle at a distance $a + L$ from the origin, with polar angle $\phi = 0$ or π , azimuthal angle θ undefined (in the same way that the longitude at the North Pole is undefined). There are only two such locations, so the available volume is limited. However, the side-by-side configuration has $\phi = \pi/2$, and all values of θ are allowed, giving an available volume that is 6.5 times larger than that of in-line configuration. The diagonal configuration, with $\phi = \pi/4$ or $3\pi/4$ and all values of θ allowed, has an available volume 9.2 times that of the in-line configuration. Of course, in a random dispersion all values of ϕ will occur, but this simple analysis makes it clear that the effects resulting from particle positions with values of ϕ near 0 or π (i.e., near the in-line configuration) should play a minor role in the scattering properties of a film, if only pairwise configurations of particles were important. However, because of the nonmonotonic behavior of the scattering as ϕ is changed, and the variation with wavelength, these statistical observations do

not lead to a simple global conclusion about the influence of pairwise interactions on scattering in a random distribution.

However, if the distribution of particles is not random, but has a preferred orientation imposed on it by some external influence in processing, then one of the effects described above may predominate. This is particularly true if arrays with long-range order are formed, such as ordered colloids or opal structures. Such structures resemble the zigzag arrangement (although extended in two directions perpendicular to the direction of the incident light, rather than just one as in these calculations). As observed above, this arrangement tends to increase the scattering efficiency (i.e., to increase S), especially at longer wavelengths, but to decrease the backscattering fraction, except at the central wavelength where the scattering is strongest. Such an arrangement, if it were to occur in a coating, would tend to modify the color of the coating by reducing the fraction of backscattered long- and short-wavelength light relative to the intermediate wavelengths. Since the reduction is more dramatic at the longer wavelengths, this would tend to give the coating a greenish cast. This modification of the diffuse reflectance is independent of any effects attributable to the ordering itself, such as the appearance of Bragg reflection of specific wavelengths.

5. Conclusions

It is clear from the results we present here that the near-field interactions between TiO_2 particles, which cannot usually be probed experimentally, nevertheless have an observable influence on the optical characteristics of a film made of such particles. Depending on the orientation of the particles with respect to the incident light, these interactions can either increase or decrease the scattering efficiency, the isotropy of the scattering, and the magnitude of the electric field within the matrix and the particles. In the mid-visible range, two particles in line increase the backscattering fraction by 28% and the scattering strength by 38% over that of a single particle, whereas if the particles are in the diagonal configuration the backscattering fraction and scattering strength are actually reduced by addition of the second particle. At shorter or longer wavelengths the

backscattering fraction is reduced regardless of the location of the second particle, by as much as 60% when five particles are arranged in the zigzag configuration. These results are surprising in that it is generally assumed that multiple scattering enhances backscattering. Simple models of multiple scattering or scattering of two particles as a single, larger particle are inadequate to explain these results. The strong variation of the near- and far-field scattering on the relative positions of the particles can reduce the hiding power of a coating and modify its color. It can also lead to nonuniform curing in stereolithography and modified threshold electric field for stimulated emission in random laser media. Manipulation of the microstructure during processing of the particle dispersion can therefore either mitigate or enhance these effects as desired.

We thank J. Mould, Jr., for computational support in implementing the finite element code and A. Miller for assistance with the Mie scattering calculations.

References

1. D. P. Fields, R. J. Buchacek, and J. G. Dickinson, "Maximum TiO_2 hiding power—the challenge," *J. Oil Colour Chem. Assoc.* **2**, 87–93 (1993).
2. G. Mie, "Beitrage zur Optik Truber Medien Speziell Kolloidaler Metallosungen," *Ann. Phys.* **25**, 377–445 (1908).
3. C. F. Bohren and D. R. Huffman, *Absorption and Scattering of Light by Small Particles* (Wiley, New York, 1983).
4. E. S. Thiele and R. H. French, "Light-scattering properties of representative, morphological rutile titania particles studied using a finite-element method," *J. Am. Ceram. Soc.* **81**, 469–479 (1998).
5. E. S. Thiele and R. H. French, "Computation of light scattering by anisotropic spheres of rutile titania," *Adv. Mater.* **10**, 1271–1276 (1998).
6. E. S. Thiele, "Light scattering by high and low contrast particulate systems," Ph.D. dissertation (Materials Science Department, University of Pennsylvania, Philadelphia, 1998).
7. L. E. McNeil and R. H. French, "Near-field scattering from red pigment particles: absorption and spectral dependence," *J. Appl. Phys.* **89**, 1898–1906 (2001).
8. M. W. Ribarsky, "Titanium dioxide (TiO_2) (rutile)," in *Handbook of the Optical Constants of Solids*, E. D. Palik, ed. (Academic, New York, 1985), pp. 795–804.
9. The MIE TAB program was obtained from A. Miller, Department of Physics, New Mexico State University, Las Cruces, New Mexico 88003 (1999), amiller@nmsu.edu.